From models to mechanisms: defects and charge trapping in amorphous silicon nitride

Hückmann, L.

1

Introduction

1.1 Overview of Amorphous Silicon Nitride and its Technological Applications

As it does not occur naturally, silicon nitride has first been synthesized by Deville and Wöhler in 1857.[1] Due to its tendency to form amorphous phases incorporating various impurities, it took several years before pure silicon nitride could be synthesized to identify its stoichiometry.[2] It consists of silicon and nitrogen in a 3:4 ratio, where each Si atom is sp^3-hybridized and hence form a tetrahedron with four surrounding N atoms, which in turn are trigonal-planar coordinated. Accordingly, the structure can be described as a network of corner-linked SiN_4 tetrahedra. Up to now, three crystalline phases have been reported (α, β, γ), all with the composition Si_3N_4. The α- and β-phases crystallize in trigonal and hexagonal unit cells ($P31c$, $P6_3/m$),[3,4] whereby the α-phase is only stable when heavily doped.[5] The γ-phase is a more recently discovered cubic high-pressure modification.[6] From its earliest synthesis, Si_3N_4's exceptional hardness and chemical inertness were apparent, though initially it was mainly regarded as an academic curiosity. Commercial interest emerged later in the 1950s, when it was explored as a wear-resistant coating for highly stressed mechanical components.[7] Around the same time, it was discovered that charge carriers injected in amorphous silicon nitride (a-Si_3N_4) are trapped extremely efficiently[8,9] — an at first surprising and still unusual phenomenon that has since opened up a multitude of technological applications.

In modern microelectronic engineering, silicon nitride (Si_3N_4) is a ubiquitous wide-bandgap dielectric distinguished by its exceptional thermal, chemical, and mechanical stability.[10–15]

These properties made it an indispensable material in advanced silicon-based device fabrication, where thin a-Si_3N_4 films are routinely incorporated into complementary metal-oxide-semiconductor (CMOS) building blocks. There, they function as gate spacers, sidewall isolation layers, etch-resistant hard masks, and durable passivation coatings that shield device surfaces from environmental degradation and ionic diffusion.[16–23] Beyond microelectronics, silicon nitride has emerged as a key material in photonic integrated circuits (PICs). Its wide optical transparency window, ranging from the visible to the mid infrared, combined with low light wave propagation loss enables tightly confined waveguides and high-quality optical components over a broad spectral range.[24–28]

Perhaps the most technologically significant property of a-Si_3N_4, however, is its unique ability to trap charge carriers with extrapolated retention times approaching 10 years at 150 °C.[29–31] This feature forms the basis for a-Si_3N_4's wide-spread usage as the charge-trapping medium in non-volatile flash memory devices.[32,33] Typical architectures for such devices are comprised of **Si**/Si**O**$_2$/Si_3**N**$_4$/Si**O**$_2$/**Si** (SONOS) and **Ta**N/**Al**$_2$**O**$_3$/Si_3**N**$_4$/Si**O**$_2$/**Si** (TANOS) stacks, where charge carriers are injected into the nitride layer.[34–39] There, they localize and remain stored also in the absence of an external bias, enabling reliable data retention even after device power-down. In practice, these memory devices operate by trapping and releasing charge carriers during write-erase cycles aided by tunneling through shallow mid-gap states. The fact that this phenomenon is particularly pronounced in a-Si_3N_4, but significantly weaker or not at all in other Si-based materials[40–42] suggests that a-Si_3N_4 plays a key role in the process. However, despite decades of intense research, the exact underlying mechanism remains unknown.

Understanding what chemical feature governs the charge trapping process is pivotal, because charge trapping and detrapping in Si_3N_4 are intimately linked to degradation mechanisms such as bias-temperature instability (BTI)[43–45] and stress-induced leakage current (SILC),[46–48] making the microscopic nature of trap states a decisive factor in long-term device performance.[49] Also, charge traps can act as recombination and scattering centers, which are detrimental for controlling the flow of charge carriers. Hence, suppressing this effect is critical for any other application when charge trapping is not explicitly desired.

More recently, a-Si_3N_4 has also been explored as an anode material for conversion-type lithium batteries. Early results suggest that it could become a pivotal component for next-

generation energy storage systems, as it offers a significantly higher specific capacity than conventional graphite electrodes while mitigating the severe volumetric expansion observed in pure silicon anodes during lithiation.[50–54] In such systems, lithium insertion proceeds through a conversion reaction rather than intercalation, leading to the formation of a Li-Si-N matrix embedded within the amorphous phase.[55–57] The electrochemical performance and cycling stability of a-Si_3N_4-based anodes appear to depend strongly on the Si:N ratio.[58,59] Although a detailed reaction mechanism has not yet been fully established, nuclear magnetic resonance (NMR) studies suggest that lithiation transforms a-Si_3N_4 into a stable Li-Si-N matrix accompanied by the formation of Si-rich SiN_x regions.[60,61] It is well established from memory-device research that amorphous silicon nitride is electronically active, with the nature and density of mid-gap states being highly sensitive to both stoichiometry and extrinsic defects. These electronic trap states, which govern charge capture and transport in microelectronic devices, may also influence the electrochemical processes in conversion-type anodes. It is therefore plausible that these phenomena in a-Si_3N_4 play a key role in conversion-type batteries.

1.2 Electronic Structure and Defect-Mediated Charge Trapping

Most of the applications discussed above either rely on or are strongly influenced by charge-trapping phenomena in a-Si_3N_4. Charge trapping refers to the capture of charge carriers, *i.e.,* electrons (e^-) or holes (h^+), in localized electronic states that contrast with the delocalized band states typically present in a solid. Once captured, carriers remain localized until they are re-emitted into delocalized states or transferred to another trap.

The trapping behavior is governed by the interplay between capture kinetics, emission kinetics, and the thermodynamic depth of the associated state. Carrier mobility in wide-bandgap insulating materials proceeds through several mechanisms,[62,63] including Shockley–Read–Hall-type thermal emission,[64] field-lowered thermal emission of Poole-Frenkel pairs,[65,66] trap-assisted tunneling, as well as photo- and non-radiative emission.[67,68] The rates of these processes depend on the energetic position of the trap relative to the band edges and to other accessible localized states as well as on the capture cross-section. For this reason, it

is common to distinguish between deep and shallow traps.[69] Deep traps lie far from the transport levels and require a substantial activation energy for emission, resulting in long carrier lifetimes. In contrast, shallow traps lie energetically close to extended states or adjacent defects, enabling rapid carrier exchange under moderate thermal conditions or modest external fields.[70–73] In the context of memory devices, an appropriate balance between deep and shallow traps is essential: Shallow traps facilitate efficient write-erase cycling, whereas overly shallow traps raise concerns regarding long-term data retention.

Understanding how local bonding environments and stoichiometry govern charge localization and transport is therefore crucial for optimizing a-Si_3N_4 across both electronic and electrochemical applications. The electronic behavior of a-Si_3N_4 is strongly influenced by its disordered bonding network and the prevalence of locally irregular atomic environments. In general, amorphous silicon nitride exhibits a wide band gap of approximately 4.2 eV to 5.4 eV,[74–76] which is smaller than that of its crystalline counterpart (around 6.0 eV[32]). Crucially, the amorphous phase is prone to charge trapping,[8,9] a property that enables its use in non-volatile flash memory devices but can be detrimental in optical and electronic applications. In photonics, trapped charges introduce absorption and scattering losses, while in CMOS devices they may act as recombination centers for free carriers with potentially catastrophic consequences for device reliability. Whether advantageous or harmful, charge trapping remains a defining feature of a-Si_3N_4 and must be understood at a microscopic level to harness or mitigate its effects.

Based on extensive electron paramagnetic resonance (EPR) studies, Robertson and others identified dangling silicon bonds, so-called *K-centers*, as the primary intrinsic electron traps in amorphous silicon nitride.[81–85] These are localized Anderson-states[86] that introduce defect levels approximately 1.7 eV below the conduction band minimum (CBM).[72,87–90] Analogous defects associated with twofold-coordinated nitrogen atoms (*N-centers*) have also been reported.[91–93] A schematic band diagram of a commonly employed MANOS stack (**m**etal-**a**lumina-**n**itride-**o**xide-**s**ilicon) is depicted in Figure 1.1a: Using Al as the gate electrode and a-SiO_2 as the tunnel oxide, the valence band maximum (VBM) and the CBM of a-Si_3N_4 are positioned between the corresponding levels of the electrodes and oxide layers. The relative energies of the N- and K-centers are such that in the absence of an external bias, the N-centers are below the Fermi level and, therefore, are occupied while the K-centers are

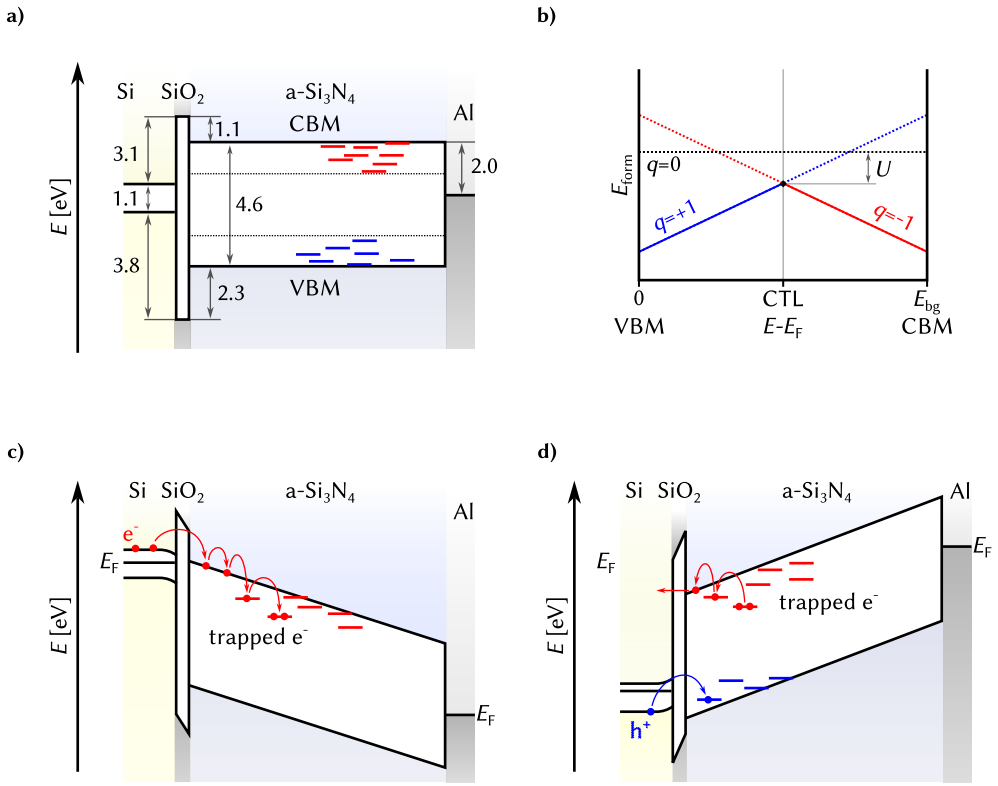

Figure 1.1: a) Band diagram of a typical MNOS-structure with a-Si_3N_4 embedded between SiO_2 and a metal electrode (here Al). The hole and electron trap precursor states are drawn in blue and red, respectively. Adapted from Reference [77]. b) Illustration of the dependence of defect formation energy (E_{form}) on the Fermi level (E_F). The intersections between lines corresponding to different charge states indicate the charge transition levels (CTLs), where one charge state becomes energetically more favorable than another. The less stable charge state acts as a donor or acceptor, depending on the direction of the transition. The energy separation between successive CTLs defines the correlation energy U. When $U < 0$, the defect exhibits negative-U behavior, favoring paired charge transitions.[78] c) Band diagram of a MNOS stack during charging/writing. d) Band diagram of a MNOS stack during discharging/erasing. Adapted from References [79, 80].

empty. Consequently, N-centers serve as precursors for holes, whereas K-centers are capable of taking up electrons. Both K- and N-centers exhibit negative-*U* behavior (Figure 1.1b), whereby the charged configuration is energetically favored over the neutral one according to[92,94]

$$K^0 + N^0 \longrightarrow K^+ + N^- \,. \tag{1.1}$$

This also implies that any charge transition occurs via a two-electron process

$$K^- \rightleftharpoons K^+ + 2\ e^- \,. \tag{1.2}$$

A write operation in the memory device is performed by applying an external electric field via the Al electrode, inducing electron tunneling through the a-SiO_2 layer into localized states within the a-Si_3N_4 layer (Figure 1.1c). Within a-Si_3N_4, electrons retain limited mobility through mechanisms described above, and charge leakage remains a concern for long-term data retention. The erase operation proceeds by reversing this process (Figure 1.1d).

Curiously, an increased concentration of EPR-active centers has been observed in Si-rich regions, motivating the use of sub-stoichiometric SiN_x films to tune trap densities and energy levels.[33,95] This raises an important question: Does the enhanced trap concentration in Si-rich compositions originate primarily from a higher density of nitrogen vacancies and associated K-centers, or do Si—Si bonds themselves contribute to the formation of trap states?

To gain deeper insight into the underlying mechanisms, extensive efforts have been devoted to the computational modeling of amorphous silicon nitride (a-Si_3N_4).[96–99] The principal bottleneck for such studies has been — and to some extent remains — the significant computational resources required. Because amorphous materials lack long-range order, large simulation cells are necessary to mitigate finite-size effects, and algorithms for generating realistic amorphous networks typically demand long molecular dynamics trajectories. This makes *ab initio* simulations computationally expensive, often requiring a brute-force approach in which potential artifacts are tolerated under the assumption that the accuracy of the electronic-structure method outweighs shortcomings in the structural model.[99,100] An alternative and more practical strategy employs a two-step procedure: Amorphous structures are first generated using classical interatomic potentials and subsequently refined and analyzed using *ab initio* methods such as density functional theory (DFT).[99,101–104]

Although neither approach completely resolves the computational challenges inherent to amorphous materials, both have yielded meaningful insights into the electronic properties of a-Si_3N_4. DFT calculations have reproduced the localized Anderson states associated with threefold-coordinated silicon atoms and confirmed their characteristic negative-U behavior.[99] Similar features, however, also arise when Si–Si bonds are present in the model,[105] leaving the question unanswered of whether experimentally observed defect states in SiN_x originate primarily from dangling bonds, Si-Si pairs, or a combination thereof.

1.3 Composition and Chemistry in Si–N–O Systems

Up to this point, the discussion has focused primarily on point defects and the intrinsic properties of pristine amorphous silicon nitride. In practical applications, however, a-Si_3N_4 rarely exists in isolation; it is typically embedded within complex multilayer stacks where interfacial interactions and impurities are unavoidable. The synthesis route itself plays a decisive role in determining the structural and electronic properties of the material. A holistic understanding of a-Si_3N_4 therefore requires consideration of its rich chemical variability and how processing conditions influence its microscopic structure and defect landscape. Most technological applications rely on amorphous thin films, partly because crystalline Si_3N_4 cannot be epitaxially grown on silicon substrates.[106] The substantial lattice mismatch and the resulting high density of grain boundaries render crystalline films mechanically and electronically unsuitable for device integration. Consistent with this, charge-trapping phenomena have not been reported in crystalline Si_3N_4. In contrast, a-Si_3N_4 can be readily deposited on silicon by chemical vapor deposition (CVD), yielding smooth, uniform thin films. Various synthesis strategies exist, but they generally rely on reactions between gaseous silicon- and nitrogen-containing precursors, such as silicon chlorides and ammonia, under controlled thermal or plasma conditions, for example:[107]

$$3\,SiCl_{4(g)} + 4\,NH_{3(g)} \longrightarrow \text{a-}Si_3N_4 \downarrow + 12\,HCl_{(g)} \tag{1.3}$$

The network of a-Si_3N_4 is built upon the same fundamental bonding motif found in other silicon-based materials such as crystalline silicon (α-Si), silicon dioxide (SiO_2), and silicon carbide (SiC). Each silicon atom is tetrahedrally coordinated by four nitrogen atoms, while

nitrogen atoms are typically threefold coordinated by silicon. Similar to amorphous silica (a-SiO_2), this arrangement forms a three-dimensional, corner-linked network of tetrahedra. However, because nitrogen has a higher valence than oxygen, a-Si_3N_4 is significantly denser and structurally more complex. In a-SiO_2, oxygen forms twofold-bridging bonds that produce a uniform and well-characterized glass network, whereas nitrogen's threefold coordination introduces additional configurational freedom. The resulting structure is denser and more rigid, with greater distortion of the coordination polyhedra and a non-negligible concentration of intrinsic defects. So overall, the structurally diverse environment shows enhanced variation in bond angles, ring statistics, and network connectivity, which lead to a wide variety in properties across Si-based compounds (Table 1.1). These features allow a-Si_3N_4 to accommodate substantial local disorder without catastrophic structural instability, yet it facilitates the formation of sub-stoichiometric bonding motifs and defects that strongly influence the electronic and functional properties of the material. Such structural adaptability is central to device engineering but also represents a fundamental source of complexity in understanding and controlling the behavior of amorphous silicon nitride.

Since Si_3N_4 and SiO_2 are not only structurally related but also frequently used in conjunction with one another, it is instructive to examine the Si-N-O phase diagram (see Figure 1.2). Although Si_3N_4 is thermodynamically less stable than SiO_2, it exhibits remarkable oxidation resistance owing to the strength of the Si-N bond and the formation of a thin protective oxide layer. In amorphous films, oxygen can be readily incorporated in virtually any N:O ratio, for instance by introducing oxygen-containing species such as NO_x into the gas mixture

Table 1.1: Overview of Si-based solids: The density ρ, bulk modulus B, defect concentration c_d, cohesive energy E_{coh}, the heat of formation $\Delta_f H$, the band gap E_{bg}, and the dielectric constant ε_r for crystalline silicon in the diamond cubic phase (α-Si), amorphous silicon (a-Si), amorphous silicon dioxide (a-SiO_2), and amorphous silicon nitride (a-Si_3N_4).

property		α-Si		a-Si		a-SiO_2		a-Si_3N_4	
ρ	$g\,cm^{-3}$	2.33	[108]	2.10	[109]	2.20	[110]	$2.6-3.0$	[9]
B	GPa	98	[111]	$71-77$	[112]	$35-40$	[113]	$150-180$	[114]
c_d	%	$\gtrsim 0$	[115]	12	[116]	$\gtrsim 0$	[117]	$23-32$	[118]
E_{coh}	$eV\,f.u.^{-1}$	4.66	[119]	4.59	[120]			$54.5-56.5$	[97]
$\Delta_f H$	$kJ\,mol^{-1}$	0.0		6.74	[120]	-902.9 ± 1.2	[121]	-760 ± 12	[122]
E_{bg}	eV	1.13	[123]	$1.5-2.0$	[124]	$8.0-10.0$	[125]	$4.2-5.4$	[76]
ε_r		11.68	[126]	11.8	[127]	3.9	[128]	$7.0-10.5$	[99]

[a] f.u. = formula unit.

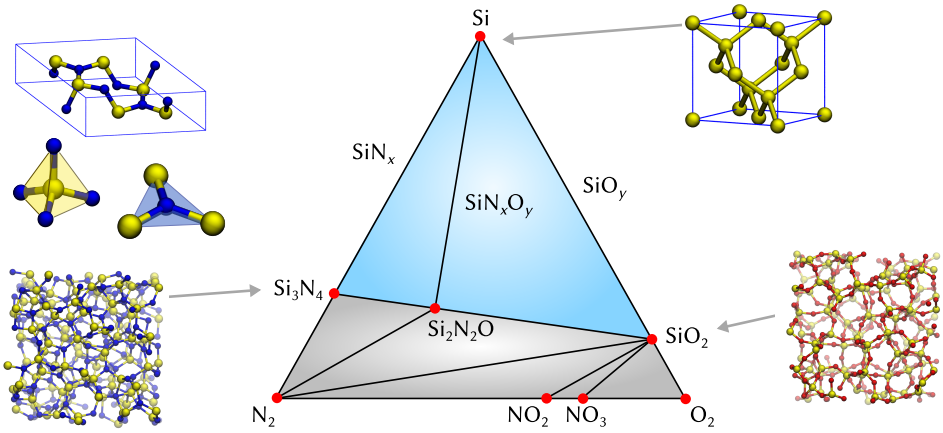

Figure 1.2: Phase diagram of the ternary Si-N-O system with the stoichiometric polymorphs are marked by red circles and are labeled. Left: crystalline β-Si_3N_4, amorphous Si_3N_4, and the coordination geometries of Si and N. Right: crystalline α-Si (diamond structure) and amorphous SiO_2. The condensed phases under ambient condition are colored blue. The gaseous phase is gray. Not true to scale for visibility.

during the CVD process. Among the ternary Si-N-O compounds, only Si_2N_2O forms a well-defined crystalline phase, but its demanding synthesis conditions and limited compositional tunability preclude widespread technological use. Oxygen impurities or mixed Si-O-N regions can also form unintentionally during high-temperature annealing of freshly deposited a-Si_3N_4 layers in semiconductor processing. In either case, the incorporation of oxygen substantially alters the electronic structure of the material:[129–134] Si–O bonds widen the band gap and can passivate defect states, while mixed bonding environments (Si–O–N) or sub-stoichiometric regions may introduce new trap levels. Consequently, oxygen incorporation can be both beneficial and detrimental, depending on the local bonding configuration and the intended device application.[134–140]

Another degree of freedom arises from the ability of silicon to bond with other silicon atoms without compromising the structural or chemical integrity of the film. Although the cohesive energy of elemental silicon is lower than that of Si_3N_4 or SiO_2 (see Table 1.1), the rigidity and low permeability of a-Si_3N_4 allow the formation of Si–Si bonds in regions of local stoichiometric imbalance.[141] In practice, synthesizing perfectly stoichiometric amorphous silicon nitride is challenging; thus, the composition is more accurately described as $SiN_{x\lesssim1.33}$. The presence of Si–Si bonds strongly influences the electronic and charge-trapping properties of the material, and increasing their concentration is often associated with enhanced

trap densities. Consequently, adjusting the Si:N ratio is a common strategy to fine-tune the electrical and optical characteristics of a-SiN_x.[142,143] Nevertheless, this thesis focuses on stoichiometric a-Si_3N_4 and addresses the challenge of modeling its structural and electronic properties at the atomic scale.

1.4 The Aim of this Thesis

In contrast to crystalline dielectrics, where symmetry constrains the defect chemistry leading to a finite set of defect states, the electronic states in amorphous Si_3N_4 arise from a broad spectrum of local structural motifs. The inherently amorphous and chemically flexible character of a-Si_3N_4 means that its electronic properties emerge from the interplay of structural disorder, local compositional variations, and charge carrier-induced relaxation. Although a-Si_3N_4 has been extensively studied and is widely used commercially, several critical questions remain unanswered. After introducing the relevant methodology in Chapter 2, this thesis addresses four key unknowns by means of state-of-the-art electronic structure calculations:

1. How can amorphous materials and defects therein be modeled? As discussed earlier, computational modeling of a-Si_3N_4 has been limited by the large system sizes and extensive configurational sampling required. Advances in high-performance and exa-scale computing gradually diminish these limitations and open up new possibilities to improve the computational modeling of amorphous materials. In Chapter 3, I present a novel methodology for systematically sampling amorphous configurations, ensuring comprehensive coverage of relevant structural and electronic descriptors. This approach is further extended to extrinsic defects, enabling efficient exploration of the configuration space while carefully tracking potential gaps in the sampling. To address the vastness of the configurational space, a hierarchical strategy is required beginning with comprehensive large-scale sampling using classical potentials followed by targeted *ab initio* calculations. To enable the former, I investigate in Chapter 4 how Bayesian optimization can be used to tailor force-field parameters for these specific applications.

2. Which chemical feature governs charge trapping? EPR and photoluminescence experiments, supported by computational models, attribute charge trapping to undercoordinated silicon. However, because trapping occurs preferentially in Si-rich regions, it remains unclear whether K-centers or Si–Si bonds are the primary origin. Critically, dangling Si bonds are inherently unstable and prone to oxidation or hydrogen passivation. Thermal annealing during device fabrication is expected to further reduce their prevalence. Nevertheless, a-Si_3N_4-based memory devices exhibit exceptional lifetimes, implying a yet-to-be-discovered mechanism that reconciles these observations. In Chapter 5, a hitherto unknown mode of intrinsic polaronic trapping of electrons in a-Si_3N_4 is identified: Charging generates a K-center or Si-Si-type defect while discharging recovers the original network structure. Thus, it is the reversible structural response of a-Si_3N_4 that allows to trap charge carriers.

3. How do external defects (H, O) affect the electronic properties? a-Si_3N_4 is often-times exposed to impurities, particularly hydrogen and oxygen, either through ion migration during annealing of SONOS stacks or as a byproduct of deposition (see Equation 1.3). These extrinsic species alter the electronic properties by modifying defect concentrations, passivating mid-gap states, and affecting mechanical stability. Understanding the chemistry of H- and O-related defects and their interaction with intrinsic mid-gap states is therefore crucial for predicting and fine-tuning material properties. Chapter 6 bridges the previously fragmented understanding of charge trapping and hydrogen incorporation. We demonstrate that hydrogen plays a dual role: It can repair coordination defects, healing the network, yet also promotes Si–N bond breaking in strained areas, thus compromising the network integrity.

4. What is the interplay between charge trapping and the initial stages of lithium incorporation? As discussed in length up to this point, the material properties of a-Si_3N_4 are highly sensitive to external defects. In particular, the edge states and therefore the trapping characteristics can change dramatically. It therefore stands to reason that these effects may also play a role when a-Si_3N_4 is employed in conversion-type anodes for next-generation Li-ion batteries. Chapter 8 demonstrates that the initial transformation of a-Si_3N_4 is controlled by charge trapping through polaron and bipolaron formation, which drives the emergence of Si-rich active regions and a stabilizing Li–Si–N matrix within the anode.

References

[1] Deville, H. É. S.-C.; Wöhler, F. *Liebigs Ann. Chem.* **1857**, *104*, 256–256.

[2] Weiss, L.; Engelhardt, T. *Z. Anorg. Allg. Chem.* **1910**, *65*, 38–104.

[3] Priest, H. F.; Burns, F. C.; Priest, G. L.; Skaar, E. C. *J. Am. Ceram. Soc.* **1973**, *56*, 395–395.

[4] Du Boulay, D.; Ishizawa, N.; Atake, T.; Streltsov, V.; Furuya, K.; Munakata, F. *Acta Crystallogr. B* **2004**, *60*, 388–405.

[5] Liang, J.-j.; Topor, L.; Navrotsky, A.; Mitomo, M. *J. Mater. Res.* **1999**, *14*, 1959–1968.

[6] Zerr, A.; Miehe, G.; Serghiou, G.; Schwarz, M.; Kroke, E.; Riedel, R.; Fueß, H.; Kroll, P.; Boehler, R. *Nature* **1999**, *400*, 340–342.

[7] Riley, F. L. *J. Am. Ceram. Soc.* **2000**, *83*, 245–265.

[8] Hu, S. M.; Kerr, D. R.; Gregor, L. V. *Appl. Phys. Lett.* **1967**, *10*, 97–99.

[9] Chu, T. L.; Szedon, J.; Lee, C. *Solid-State Electron.* **1967**, *10*, 897–905.

[10] Meena, J. S.; Sze, S. M.; Chand, U.; Tseng, T.-Y. *Nanoscale Res. Lett.* **2014**, *9*, 526.

[11] Barta, J.; Manela, M.; Fischer, R. *Mater. Sci. Eng.* **1985**, *71*, 265–272.

[12] Li, X.; Yin, X.; Zhang, L.; Cheng, L.; Qi, Y. *Mater. Sci. Eng. A* **2009**, *500*, 63–69.

[13] Du, H.; Li, Y.; Cao, C. *J. Alloys Compd.* **2010**, *503*, L9–L13.

[14] Vila, M.; Cáceres, D.; Prieto, C. *J. Appl. Phys.* **2003**, *94*, 7868.

[15] Dong, X.; Wu, J.; Yu, H.; Zhou, Q.; Wang, W.; Zhang, X.; Zhang, L.; Li, L.; He, R. *Int. J. Appl. Ceram. Technol.* **2022**, *19*, 2929–2949.

[16] Liu, H.-W.; Su, H.-P.; Lai, W.-K.; Cheng, H.-C. *J. Electrochem. Soc.* **1997**, *144*, 3288.

[17] Wrazien, S. J.; Zhao, Y.; Krayer, J. D.; White, M. H. *Solid State Electron.* **2003**, *47*, 885–891.

[18] Wang, L.; Yang, C.-H.; Wen, J. *Electron. Mater. Lett.* **2015**, *11*, 505–543.

[19] Doo, V. Y.; Nichols, D. R.; Silvey, G. A. *J. Electrochem. Soc.* **1966**, *113*, 1279.

[20] Okada, Y.; Tokumaru, Y. *J. Appl. Phys.* **1984**, *56*, 314–320.

[21] Törmä, P. T.; Sipilä, H. J.; Mattila, M.; Kostamo, P.; Kostamo, J.; Kostamo, E.; Lipsanen, H.; Nelms, N.; Shortt, B.; Bavdaz, M.; Laubis, C. *IEEE Trans. Nuc. Sci.* **2013**, *60*, 1311–1314.

[22] Törmä, P. T.; Kostamo, J.; Sipilä, H.; Mattila, M.; Kostamo, P.; Kostamo, E.; Lipsanen, H.; Laubis, C.; Scholze, F.; Nelms, N.; Shortt, B.; Bavdaz, M. *IEEE Trans. Nuc. Sci.* **2014**, *61*, 695–699.

[23] Cornaby, S.; Bilderback, D. H. *J. Sync. Rad.* **2008**, *15*, 371–373.

[24] Sacher, W. D.; Huang, Y.; Ding, L.; Barwicz, T.; Mikkelsen, J. C.; Taylor, B. J. F.; Lo, G.-Q.; Poon, J. K. S. *Opt. Express* **2014**, *22*, 11167.

[25] Blumenthal, D. J.; Heideman, R.; Geuzebroek, D.; Leinse, A.; Roeloffzen, C. *Proc. IEEE* **2018**, *106*, 2209–2231.

[26] Bose, D.; Harrington, M. W.; Isichenko, A.; Liu, K.; Wang, J.; Chauhan, N.; Newman, Z. L.; Blumenthal, D. J. *Light Sci. Appl.* **2024**, *13*, 156.

[27] Sharma, T.; Wang, J.; Kaushik, B. K.; Cheng, Z.; Kumar, R.; Wei, Z.; Li, X. *IEEE Access* **2020**, *8*, 195436–195446.

[28] Xiang, C.; Jin, W.; Bowers, J. E. *Photonics Res.* **2022**, *10*, A82–A96.

[29] Lina, S. H.; Chin, A.; Yeh, F. S.; McAlister, S. P. In *2008 IEEE International Electron Devices Meeting*, IEEE: San Francisco, CA, USA, 2008.

[30] Shaposhnikov, A.; Petrov, I.; Gritsenko, V.; Kim, C. *Phys. Solid State* **2007**, *49*, 1628–1632.

[31] Gismatulin, A. A.; Kamaev, G. N.; Kruchinin, V. N.; Gritsenko, V. A.; Orlov, O. M.; Chin, A. *Sci. Rep.* **2021**, *11*, 2417.

[32] Tsai, S.-J.; Wang, C.-L.; Lee, H.-C.; Lin, C.-Y.; Chen, J.-W.; Shiu, H.-W.; Chang, L.-Y.; Hsueh, H.-T.; Chen, H.-Y.; Tsai, J.-Y., et al. *Sci. Rep.* **2016**, *6*, 28326.

[33] Gritsenko, V. A.; Kruchinin, V. N.; Prosvirin, I. P.; Novikov, Y. N.; Chin, A.; Volodin, V. A. *J. Exp. Theor. Phys.* **2019**, *129*, 924–934.

[34] Herrmann, M.; Schenk, A. *J. Appl. Phys.* **1995**, *77*, 4522–4540.

[35] Arreghini, A.; Driussi, F.; Vianello, E.; Esseni, D.; van Duuren, M. J.; Golubovic, D. S.; Akil, N.; van Schaijk, R. *IEEE Trans. Electron Devices* **2008**, *55*, 1211–1219.

[36] Lu, C.-Y. *J. Nanosci. Nanotechnol.* **2012**, *12*, 7604–7618.

[37] Nam, K.-R.; Jeong, J.-K.; Sung, J.-Y.; Lee, G.-W. *Trans. Electr. Electron. Mater.* **2021**, *22*, 372–377.

[38] Choi, S.; Lim, Y.; Kim, S.; Park, S.; Ku, B.; Kim, H.; Yang, J.; Kim, B.; Son, Y.; Choi, H.; Choi, C. *Adv. Electron. Mater.* **2025**, *11*, e00960.

[39] Lee, I.; Na, J. W.; Kwak, K.; An, J. B.; Kim, H. J. *Appl. Surf. Sci. Adv.* **2025**, *29*, 100839.

[40] Nissan-Cohen, Y.; Shappir, J.; Frohman-Bentchkowsky, D. *J. Appl. Phys.* **1985**, *58*, 2252–2261.

[41] Son, N. T.; Ivanov, I. G. *J. Appl. Phys.* **2021**, *129*, 215702.

[42] Schleich, C.; Waldhoer, D.; Waschneck, K.; Feil, M. W.; Reisinger, H.; Grasser, T.; Waltl, M. *IEEE Trans. Electron Devices* **2021**, *68*, 4016–4021.

[43] Jeppson, K. O.; Svensson, C. M. *J. Appl. Phys.* **1977**, *48*, 2004–2014.

[44] Islam, A. E.; Kufluoglu, H.; Varghese, D.; Mahapatra, S.; Alam, M. A. *IEEE Trans. Electron Devices* **2007**, *54*, 2143–2154.

[45] Grasser, T.; Kaczer, B.; Goes, W.; Aichinger, T.; Hehenberger, P.; Nelhiebel, M. In *2009 IEEE International Reliability Physics Symposium*, 2009, pp 33–44.

[46] Yasuda, H.; Ikeda, N.; Ham, K.; Takagi, M.; Yoshii, I. In *Proceedings of 1994 IEEE International Reliability Physics Symposium*, 1994, pp 225–231.

[47] DiMaria, D. J.; Cartier, E. *J. Appl. Phys.* **1995**, *78*, 3883–3894.

[48] Gritsenko, V. A.; Gismatulin, A. A.; Baraban, A. P.; Chin, A. *Mater. Res. Express* **2019**, *6*, 076401.

[49] Kim, S. S.; Yong, S. K.; Kim, W.; Kang, S.; Park, H. W.; Yoon, K. J.; Sheen, D. S.; Lee, S.; Hwang, C. S. *Adv. Mater.* **2023**, *35*, 2200659.

[50] Wu, C.-Y.; Chang, C.-C.; Duh, J.-G. *J. Power Sources* **2016**, *325*, 64–70.

[51] Li, P.; Zhao, G.; Zheng, X.; Xu, X.; Yao, C.; Sun, W.; Dou, S. X. *Energy Storage Mater.* **2018**, *15*, 422–446.

[52] Ham, S. Y.; Sebti, E.; Cronk, A.; Pennebaker, T.; Deysher, G.; Chen, Y. T.; Oh, J. A. S.; Lee, J. B.; Song, M. S.; Ridley, P.; Tan, D. H.; Clément, R. J.; Jang, J.; Meng, Y. S. *Nat. Commun.* **2024**, *15*, 1–9.

[53] Obrovac, M. N.; Chevrier, V. L. *Chem. Rev.* **2014**, *114*, 11444–11502.

[54] Huo, H.; Jiang, M.; Bai, Y.; Ahmed, S.; Volz, K.; Hartmann, H.; Henss, A.; Singh, C. V.; Raabe, D.; Janek, J. *Nat. Mater.* **2024**, *23*, 543–551.

[55] Ulvestad, A.; Skare, M. O.; Foss, C. E.; Krogsæter, H.; Reichstein, J. F.; Preston, T. J.; Mæhlen, J. P.; Andersen, H. F.; Koposov, A. Y. *ACS Nano* **2021**, *15*, 16777–16787.

[56] Bai, S. et al. *Adv. Energy Mater.* **2023**, *13*, 2301041.

[57] Obrovac, M. N.; Christensen, L. *Electrochem. Solid-State Lett.* **2004**, *7*, A93–A96.

[58] Ulvestad, A.; Mæhlen, J. P.; Kirkengen, M. *J. Power Sources* **2018**, *399*, 414–421.

[59] Ulvestad, A.; Andersen, H. F.; Jensen, I. J.; Mongstad, T. T.; Mæhlen, J. P.; Prytz, Ø.; Kirkengen, M. *Sci. Rep.* **2018**, *8*, 8634.

[60] Kilian, S. O.; Wankmiller, B.; Sybrecht, A. M.; Twellmann, J.; Hansen, M. R.; Wiggers, H. *Adv. Mater. Interfaces* **2022**, *9*, 2201389.

[61] Lovett, A. J.; Füredi, M.; Bird, L.; Said, S.; Frost, B.; Shearing, P. R.; Guldin, S.; Miller, T. S. *ACS Electrochem.* **2025**, *1*, 962–973.

[62] Grasser, T. *Microelectron. Reliab.* **2012**, *52*, 39–70.

[63] Sze, S. M.; Li, Y.; Ng, K. K., *Physics of Semiconductor Devices*, 4th ed.; John Wiley & Sons, Inc: Hoboken, NJ, 2021.

[64] Shockley, W.; Read, W. T. *Phys. Rev.* **1952**, *87*, 835–842.

[65] Stratton, R. *Phys. Rev.* **1962**, *125*, 67–82.

[66] Ralph, S. E.; Grischkowsky, D. *Appl. Phys. Lett.* **1991**, *59*, 1972–1974.

[67] Huang, K.; Rhys, A. *Proc. R. Soc. Lond. A: Math. Phys. Sci.* **1950**, *204*, 406–423.

[68] Alkauskas, A.; McCluskey, M. D.; Van de Walle, C. G. *J. Appl. Phys.* **2016**, *119*, 181101.

[69] Peaker, A. R.; Markevich, V. P.; Coutinho, J. *J. Appl. Phys.* **2018**, *123*, 161559.

[70] Strand, J.; Kaviani, M.; Gao, D.; El-Sayed, A.-M.; Afanas'ev, V. V.; Shluger, A. L. *J. Phys.: Condens. Matter* **2018**, *30*, 233001.

[71] Haneef, H. F.; Zeidell, A. M.; Jurchescu, O. D. *J. Mater. Chem. C* **2020**, *8*, 759–787.

[72] Lundkvist, L.; Lundström, I.; Svensson, C. *Solid-State Electron.* **1973**, *16*, 811–823.

[73] Vishnyakov, A. V.; Novikov, Y.; Gritsenko, V. A.; Nasyrov, K. A. *Solid State Electron.* **2009**, *53*, 251–255.

[74] Iqbal, A.; Jackson, W. B.; Tsai, C. C.; Allen, J. W.; Bates Jr., C. W. *J. Appl. Phys.* **1987**, *61*, 2947–2954.

[75] Carson, R. D.; Schnatterly, S. E. *Phys. Rev. B* **1986**, *33*, 2432–2438.

[76] Resende, J.; Fuard, D.; Le Cunff, D.; Tortai, J.-H.; Pelissier, B. *Mater. Chem. Phys.* **2021**, *259*, 124000.

[77] Novikov, Y. N.; Gritsenko, V. A. *J. Appl. Phys.* **2024**, *136*, 014101.

[78] Watkins, G. D. In *Advances in Solid State Physics: Plenary Lectures of the 48th Annual Meeting of the German Physical Society (DPG)*, Grosse, P., Ed.; Springer: Berlin, Heidelberg, 1984, pp 163–189.

[79] Sze, S. M.; Li, Y.; Ng, K. K., *Physik der Halbleiterbauelemente*, 1st ed.; Wiley-VCH: Weinheim, 2021.

[80] Novikov, Y. N.; Gritsenko, V. A. *J. Non-Cryst. Solids* **2020**, *544*, 120186.

[81] Robertson, J.; Powell, M. J. *Appl. Phys. Lett.* **1984**, *44*, 415–417.

[82] Warren, W. L.; Lenahan, P. M. *Phys. Rev. B* **1990**, *42*, 1773–1780.

[83] Robertson, J. *Philos. Mag., B* **1991**, *63*, 47–77.

[84] Warren, W.; Robertson, J.; Kanicki, J. *Appl. Phys. Lett.* **1993**, *63*, 2685–2687.

[85] Krick, D. T.; Lenahan, P. M.; Kanicki, J. *Phys. Rev. B* **1988**, *38*, 8226–8229.

[86] Anderson, P. W. *Phys. Rev.* **1958**, *109*, 1492.

[87] Nasyrov, K. A.; Gritsenko, V. A.; Novikov, Y. N.; Lee, E.-H.; Yoon, S. Y.; Kim, C. W. *J. Appl. Phys.* **2004**, *96*, 4293–4296.

[88] Lusky, E.; Shacham-Diamand, Y.; Shappir, A.; Bloom, I.; Eitan, B. *Appl. Phys. Lett.* **2004**, *85*, 669–671.

[89] Wang, Y.; White, M. H. *Solid State Electron.* **2005**, *49*, 97–107.

[90] Tzeng, S.-D.; Gwo, S. *J. Appl. Phys.* **2006**, *100*, 023711.

[91] Warren, W. L.; Lenahan, P. M.; Curry, S. E. *Phys. Rev. Lett.* **1990**, *65*, 207–210.

[92] Warren, W.; Kanicki, J.; Rong, F.; Poindexter, E. *J. Electrochem. Soc.* **1992**, *139*, 880.

[93] Warren, W. L.; Kanicki, J.; Poindexter, E. H. *Colloids Surf. A: Physicochem. Eng. Asp.* **1996**, *115*, 311–317.

[94] Lenahan, P.; Krick, D.; Kanicki, J. *Appl. Surf. Sci.* **1989**, *39*, 392–405.

[95] Petersen, M.; Roizin, Y. *Appl. Phys. Lett.* **2006**, *89*, 053511.

[96] Vianello, E. et al. In *2009 IEEE International Electron Devices Meeting (IEDM)*, IEEE: Baltimore, MD, USA, 2009.

[97] Vedula, R. P.; Anderson, N. L.; Strachan, A. *Phys. Rev. B* **2012**, *85*, 205209.

[98] Di Valentin, C.; Palma, G.; Pacchioni, G. *J. Phys. Chem. C* **2011**, *115*, 561–569.

[99] Kang, G.; Lee, D.; Lee, K.; Kim, J.; Han, S. *Phys. Rev. Appl.* **2018**, *10*, 064052.

[100] Hintzsche, L.; Fang, C.; Watts, T.; Marsman, M.; Jordan, G.; Lamers, M.; Weeber, A.; Kresse, G. *Phys. Rev. B* **2012**, *86*, 235204.

[101] Adabifiroozjaei, E.; Mofarah, S. S.; Ma, H.; Jiang, Y.; Assadi, M. H. N.; Suzuki, T. S. *Comput. Mater. Sci.* **2020**, *178*, 109632.

[102] Dasmahapatra, A.; Kroll, P. *Comput. Mater. Sci.* **2018**, *148*, 165–175.

[103] Marian, C. M.; Gastreich, M.; Gale, J. D. *Phys. Rev. B* **2000**, *62*, 3117–3124.

[104] Chen, X.; Wang, Y.-W.; Liu, X.; Wang, X.-B.; Zhao, Y.-Q. *J. Non-Cryst. Solids* **2015**, *414*, 1–6.

[105] Gritsenko, V. A.; Nekrashevich, S. S.; Vasilev, V. V.; Shaposhnikov, A. V. *Microelectron. Eng.* **2009**, *86*, 1866–1869.

[106] Wang, X.-S. *Phys. Rev. B* **1999**, *60*, R2146–R2149.

[107] Mazdiyasni, K. S.; Cooke, C. M. *J. Am. Ceram. Soc.* **1973**, *56*, 628–633.

[108] Arblaster, J. W., *Selected Values of the Crystallographic Properties of the Elements*, 1st ed.; ASM International: Materials Park, Ohio, 2018.

[109] Custer, J. S.; Thompson, M. O.; Jacobson, D. C.; Poate, J. M.; Roorda, S.; Sinke, W. C.; Spaepen, F. *Appl. Phys. Lett.* **1994**, *64*, 437–439.

[110] Tsiok, O. B.; Brazhkin, V. V.; Lyapin, A. G.; Khvostantsev, L. G. *Phys. Rev. Lett.* **1998**, *80*, 999–1002.

[111] Masolin, A.; Bouchard, P.-O.; Martini, R.; Bernacki, M. *J. Mater. Sci.* **2013**, *48*, 979–988.

[112] Kuschnereit, R.; Fath, H.; Kolomenskii, A. A.; Szabadi, M.; Hess, P. *Appl. Phys. A* **1995**, *61*, 269–276.

[113] Deschamps, T.; Margueritat, J.; Martinet, C.; Mermet, A.; Champagnon, B. *Sci. Rep.* **2014**, *4*, 7193.

[114] Khan, A.; Philip, J.; Hess, P. *J. Appl. Phys.* **2004**, *95*, 1667–1672.

[115] Sanders, I. R.; Dobson, P. S. *Philos. Mag.* **1969**, *20*, 881–893.

[116] Laaziri, K.; Kycia, S.; Roorda, S.; Chicoine, M.; Robertson, J. L.; Wang, J.; Moss, S. C. *Phys. Rev. B* **1999**, *60*, 13520–13533.

[117] Skuja, L.; Hirano, M.; Hosono, H.; Kajihara, K. *Phys. Status Solidi (C)* **2005**, *2*, 15–24.

[118] Misawa, M.; Fukunaga, T.; Niihara, K.; Hirai, T.; Suzuki, K. *J. Non-Cryst. Solids* **1979**, *34*, 313–321.

[119] Farid, B.; Godby, R. W. *Phys. Rev. B* **1991**, *43*, 14248–14250.

[120] Kail, F.; Farjas, J.; Roura, P.; Secouard, C.; Nos, O.; Bertomeu, J.; Cabarrocas, P. R. i. *Phys. Status Solidi Rapid Res. Lett.* **2011**, *5*, 361–363.

[121] Rand, M.; Palmer, D. A.; Fuger, J.; Gajda, T., *Chemical Thermodynamics of Selected Ancillary Compounds of Interest to Radioactive Waste Management*, 1st ed.; Chemical Thermodynamics, Vol. 15; OECD Nuclear Energy Agency: Boulogne-Billancourt, France, 2024.

[122] Tomaszkiewicz, I. *J. Therm. Anal. Calorim.* **2001**, *65*, 425–433.

[123] Bludau, W.; Onton, A.; Heinke, W. *J. Appl. Phys.* **1974**, *45*, 1846–1848.

[124] Futako, W.; Kamiya, T.; Fortmann, C. M.; Shimizu, I. *J. Non-Cryst. Solids* **2000**, *266-269*, 630–634.

[125] Bosio, C.; Czaja, W. *Europhys. Lett.* **1993**, *24*, 197.

[126] Dunlap, W. C.; Watters, R. L. *Phys. Rev.* **1953**, *92*, 1396–1397.

[127] McGuire, G. E., *Semiconductor Materials and Process Technology Handbook: For Very Large Scale Integration (VLSI) and Ultra Large Scale Integration (ULSI)*; Materials Science and Process Technology Series; Noyes Publications: Park Ridge, N.J., U.S.A, 1988.

[128] Gray, P. R., *Analysis and Design of Analog Integrated Circuits*, 5th ed.; Wiley: New York, 2009.

[129] Kapoor, V. J.; Bailey, R. S.; Smith, S. R. *J. Vac. Sci. Technol.* **1981**, *18*, 305–308.

[130] Xu, D.; Kapoor, V. J. *J. Appl. Phys.* **1991**, *70*, 1570–1574.

[131] Yeh, J.-l.; Lee, S.-C. *J. Appl. Phys.* **1996**, *79*, 656–663.

[132] Gritsenko, V. A.; Wong, H.; Xu, J. B.; Kwok, R. M.; Petrenko, I. P.; Zaitsev, B. A.; Morokov, Y. N.; Novikov, Y. N. *J. Appl. Phys.* **1999**, *86*, 3234–3240.

[133] Karakolis, P.; Normand, P.; Dimitrakis, P.; Sygelou, L.; Ntinas, V.; Fyrigos, I. A.; Karafyllidis, I.; Sirakoulis, G. C. In *2019 IEEE/ACM International Symposium on Nanoscale Architectures (NANOARCH)*, IEEE: Qingdao, China, 2019, pp 1–2.

[134] Vasileiadis, N.; Karakolis, P.; Mandylas, P.; Ioannou-Sougleridis, V.; Normand, P.; Perego, M.; Komninou, P.; Ntinas, V.; Fyrigos, I.-A.; Karafyllidis, I.; Sirakoulis, G. C.; Dimitrakis, P. *IEEE Trans. Nanotechnol.* **2021**, *20*, 356–364.

[135] Sandhya, C.; Oak, A. B.; Chattar, N.; Joshi, A. S.; Ganguly, U.; Olsen, C.; Seutter, S. M.; Date, L.; Hung, R.; Vasi, J.; Mahapatra, S. *IEEE Trans. Electron Devices* **2009**, *56*, 3123–3132.

[136] You, J. H.; Kim, H. W.; Kim, D. H.; Kim, T. W.; Lee, K. W. In *2011 International Conference on Simulation of Semiconductor Processes and Devices*, IEEE: Osaka, Japan, 2011, pp 199–202.

[137] Chen, D.; Huang, S.; He, L. *J. Semicond.* **2017**, *38*, 043002.

[138] Perevalov, T. V.; Volodin, V. A.; Kamaev, G. N.; Gismatulin, A. A.; Cherkova, S. G.; Prosvirin, I. P.; Astankova, K. N.; Gritsenko, V. A. *J. Non-Cryst. Solids* **2022**, *598*, 121925.

[139] Novikov, Y. N.; Kamaev, G. N.; Prosvirin, I. P.; Gritsenko, V. A. *Appl. Phys. Lett.* **2023**, *122*, 232903.

[140] Ermak, K.; Kamaev, G.; Volodin, V. In *2025 IEEE 26th International Conference of Young Professionals in Electron Devices and Materials (EDM)*, IEEE: Altai, Russian Federation, 2025, pp 70–73.

[141] Makino, T. *J. Electrochem. Soc.* **1983**, *130*, 450.

[142] Dehan, E.; Temple-Boyer, P.; Henda, R.; Pedroviejo, J. J.; Scheid, E. *Thin Solid Films* **1995**, *266*, 14–19.

[143] Xiong, W.; Jiang, H.; Li, T.; Zhang, P.; Xu, Q.; Zhao, X.; Wang, G.; Liu, Y.; Luo, Y.; Li, Z.; Li, J.; Yu, J.; Chao, Z.; Wang, W.; Radamson, H. H. *J. Mater. Sci.: Mater. Electron.* **2020**, *31*, 90–97.